Ionics (2021) 27:3259–3269
https://doi.org/10.1007/s11581-021-04113-x

ORIGINAL PAPER

Hydrothermal synthesis of olivine phosphates in the presence of excess phosphorus: a case study of $LiMn_{0.8}Fe_{0.19}Mg_{0.01}PO_4$

Xu Chu[1,2,3] · Wei Chen[1,2,3] · Haisheng Fang[1,2,3]

Received: 6 April 2021 / Revised: 17 May 2021 / Accepted: 19 May 2021 / Published online: 17 June 2021

Abstract

Our previous work reported a new strategy based on a P excess reaction system to hydrothermally synthesize lithium transition metal phosphates ($LiMPO_4$), and herein the effect of P excess on the synthesis and property of $LiMPO_4$ is investigated in detail by taking the multi-component $LiMn_{0.8}Fe_{0.19}Mg_{0.01}PO_4$ as a case. The results show that a proper degree of P excess is fairly profitable for hydrothermal synthesis including the effect on suppressing the occurrence of undesired Fe^{2+} oxidation during synthesis and improving the particle dispersion of hydrothermal product, and thus the obtained samples have enhanced electrochemical performance. These effects of P excess should be general and applicable to hydrothermal synthesis of other lithium transition metal phosphates.

Keywords Lithium-ion batteries · Hydrothermal synthesis · Cathode materials · $LiMnPO_4$ · P excess

Introduction

Synthesis is of fundamental importance for materials research and application, and the structure and property of a material will depend on how it is synthesized. Hydrothermal synthesis is known as a powerful process widely utilized to prepare various functional materials [1–4], because it can prepare crystalline powders directly from the solution at substantially lower temperatures without the need of post-heat treatment, and moreover the powder structure and property such as phase composition, particle size, and morphology can be flexibly tuned by controlling the hydrothermal synthesis conditions. Owing to these advantages, hydrothermal synthesis has become a common way to prepare cathode materials for lithium-ion batteries [5–10], especially the olivine lithium transition metal phosphates ($LiMPO_4$, M = Fe, Mn, Ni, Co) which are one of the three types of cathode materials in practical use [11–32]. As early as the year 2001, Whittingham's Group [33] initiated the synthesis of $LiFePO_4$ by a hydrothermal reaction and thereafter considerable works have been devoted to the hydrothermal synthesis of $LiMPO_4$ and their derivates [34–45], and the strategy for hydrothermal synthesis was always based on a Li excess reaction system for nearly two decades [6, 33–41, 46–49]. It was not until the year 2019 that our group communicated a new strategy based on a P excess reaction system to hydrothermally synthesize $LiMPO_4$ [50]. We demonstrated that $LiMPO_4$ could be hydrothermally synthesized in the P excess reaction system and could give competitive electrochemical performance. In addition, our report preliminarily showed that the hydrothermal synthesis and property of $LiMPO_4$ was apparently affected by the degree of P excess in the reaction system, which deserves further detailed studies to better understand the chemistry of this new hydrothermal synthesis based on a P excess reaction system. Therefore, in this paper, a multi-component $LiMn_{0.8}Fe_{0.19}Mg_{0.01}PO_4$ whose electrochemical performance is particularly promising as a cathode material as demonstrated by our previous works [24–26] is hydrothermally synthesized in the P excess reaction system as a case study and the effect of the degree of P excess was investigated in detail.

✉ Haisheng Fang
hsfang1981@hotmail.com

1 Key Laboratory of Advanced Battery Materials of Yunnan Province, Kunming University of Science and Technology, Kunming 650093, China

2 Key Laboratory of Nonferrous Metals Vacuum Metallurgy of Yunnan Province, Kunming University of Science and Technology, Kunming 650093, China

3 Faculty of Metallurgy and Energy Engineering, Kunming University of Science and Technology, Kunming 650093, China

Experimental

A series of $LiMn_{0.8}Fe_{0.19}Mg_{0.01}PO_4$ samples were hydrothermally synthesized with various P excess (The molar ratios of Li/M/P are 1:1:1.0, 1:1:1.2, 1:1:1.4, 1:1:1.6, 1:1:1.8, and 1:1:2.0, respectively, and M stands for metal ions.). Metal sulfates at 0.03 mol ($MnSO_4{\cdot}H_2O$ (≥ 99%), $FeSO_4{\cdot}7H_2O$ (≥ 99%), and $MgSO_4{\cdot}7H_2O$ (≥ 99%) with a molar ratio of 0.8:0.19:0.01) were firstly dissolved in 20 ml deionized water, and then the solutions of K_2HPO_4 (≥ 98%, 0.03 ~ 0.06 mol K_2HPO_4 dissolved in 20 ml deionized water) and LiOH (0.03 mol $LiOH{\bullet}H_2O$ (≥ 95%) dissolved in 20 ml deionized water) were orderly added drop by drop and thereafter stirred continuously for 1 h. The suspension for hydrothermal reaction was prepared in the nitrogen-filled glove box, and then the obtained suspension was transferred into Teflon-lined stainless steel autoclaves and heated at 200 °C for 10 h. The precipitated products were filtrated and fully washed with deionized water and finally dried at 80 °C in vacuum. To prepare $LiMn_{0.8}Fe_{0.19}Mg_{0.01}PO_4$/C composite, the hydrothermally synthesized $LiMn_{0.8}Fe_{0.19}Mg_{0.01}PO_4$ was mixed with sucrose (a nominal carbon content of 10 wt.% in the final products) by ball milling, and the obtained mixture was heated at 750 °C for 1 h under a nitrogen atmosphere.

The crystalline structures of the as-prepared $LiMn_{0.8}Fe_{0.19}Mg_{0.01}PO_4$ samples were identified by X-ray diffraction (XRD, TTR18kW, Japan) utilizing CuKα radiation. Lattice parameters were calculated by fitting the XRD patterns using JADE with peak positions calibrated by internal standard of silicon. Raman spectroscopy was measured using a Reinshaw in Via Raman microscopy with an Ar 514.5-nm laser as excitation source. The particle morphology and size of samples were observed by field-emission scanning electron microscopy (FE-SEM, Nova-Nano SEM450). The pH value of suspension was tested by a pH meter (PHBJ-260, INESA). The residual carbon content of samples was determined by a C-S Analyzer (COREY-150C, China).

Electrochemical performance of samples was assessed using CR2025 coin cells with a lithium metal anode. The cathode was made by mixing $LiMn_{0.8}Fe_{0.19}Mg_{0.01}PO_4$/C, Super P, and polyvinylidene fluoride (PVDF) in a weight ratio of 8:1:1 in *N*-methyl pyrrolidinone (NMP) to form a homogenous slurry, which was coated on an aluminum foil by a doctor blade coater and dried at 80 °C in vacuum. The electrolyte was 1 M $LiPF_6$ in EC/EMC/DMC (1:1:1 in volume) solution. All cells were assembled in an argon-filled glove box. Cells were charged at a constant current-constant voltage (CC–CV) mode and then discharged at a constant current using a battery test system (Land CT2001A). Electrochemical impedance spectroscopy (EIS) was carried out on an electrochemical workstation (Princeton Applied Research, AMETEK) in a frequency range from100 kHz to 0.01 Hz with an AC signal of 0.5 mV. All electrochemical tests were conducted at 30 °C.

Fig. 1 The suspensions after hydrothermal synthesis with various molar ratios of Li/M/P: **a** 1:1:1.0, **b** 1:1:1.2, **c** 1:1:1.4, **d** 1:1:1.6, **e** 1:1:1.8, and **f** 1:1:2.0

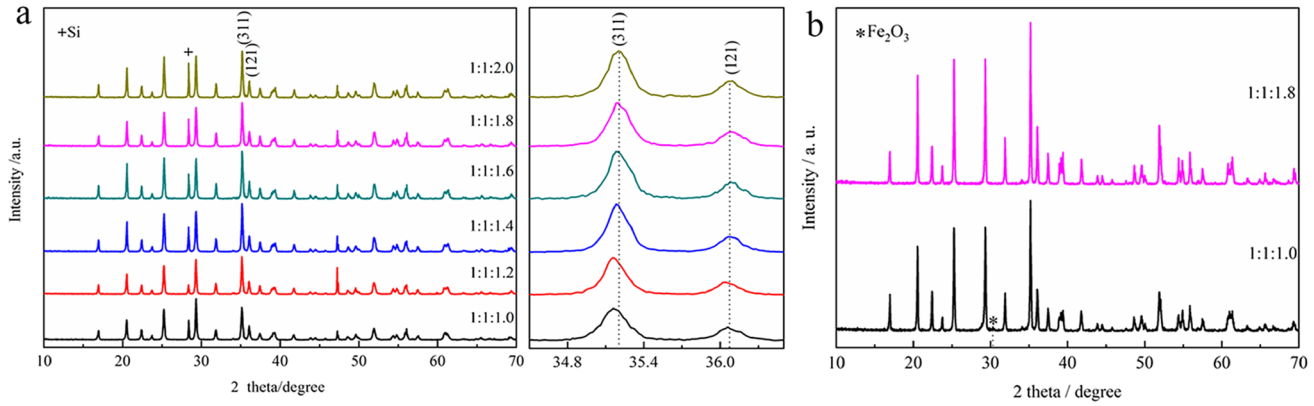

Fig. 2 **a** XRD patterns of samples hydrothermally synthesized with various molar ratios of Li/M/P and **b** XRD patterns of samples post-annealed at 600 °C for 1 h under a nitrogen atmosphere

Results and discussion

Figure 1 shows representative photos of suspensions after hydrothermal synthesis with different Li/M/P molar ratios. With increasing the P excess, the suspension color gradually changed from yellowish brown to milky white. This indicates the occurrence of undesirable oxidation reaction, and the brown color of the suspension indicates oxidative surrounding. The XRD patterns of samples hydrothermally synthesized with various molar ratios of Li/M/P are displayed in Fig. 2a. It can be seen that all samples are highly crystallized and can be identified as an orthorhombic structure with a space group of *Pnma*, and no obvious impurity peaks are found. Two samples with Li/M/P molar ratios of 1:1:1.0 and 1:1:1.8 were post-annealed at 600 °C for 1 h under a nitrogen atmosphere and further analyzed by XRD, as shown in Fig. 2b. A tiny diffraction peak of Fe_2O_3 impurity phase (indicated by asterisk) can be observed in the pattern of the post-annealed sample with a Li/M/P molar ratio of 1:1:1.0, while impurity peaks are still not found in the pattern of the post-annealed sample with a Li/M/P molar ratio of 1:1:1.8. For the hydrothermal synthesis of $LiMPO_4$ [38], the reaction was often performed in a solution under weakly acidic to weakly basic conditions ($6 < pH < 10$). The similar phenomena are observed within this research, as shown in Table 1. When the Li/M/P molar ratio is 1:1:1.0, the pH value of reaction suspensions before hydrothermal synthesis is greater than 10. Therefore, for impurities, it is most probably that during hydrothermal synthesis, Fe^{2+} oxidizes to FeO(OH), not to Fe_2O_3, that on further heating converts to Fe_2O_3. However, it is certain that undesirable oxidation reaction (Fe^{2+} oxidation) indeed occurred in the hydrothermal reaction system without P excess, and the formed oxide impurity was present in an amorphous state in the hydrothermal sample. These observations also indicate that the undesirable oxidation reaction can be suppressed by increasing P excess. Turning our attention to Fig. 2a again, it is seen that increasing P excess also results in an obvious shift of diffraction peaks to higher angle at first and then the shift becomes less obvious (peaks positions have been calibrated by internal standard of silicon). The shift of diffraction peaks indicates the variation in lattice parameters, and the result of calculated lattice parameters is listed in Table 1. It is seen that the lattice volume decreases with increasing P excess, and this change becomes less obvious when the molar ratio of Li/M/P increases to 1:1:1.6. As the sixfold-coordinated ionic radius of Fe^{2+} (0.74 Å) is smaller than that of Mn^{2+} (0.80 Å), the decreased lattice parameters mean that more Fe^{2+} was incorporated into the crystal and less impurity was formed with increasing P excess, which also demonstrates that the occurrence of undesirable oxidation is suppressed at large P excess. In addition to the structural characterization, the morphology of hydrothermal samples was observed by SEM, as shown in Fig. 3. It is seen that particles of the sample synthesized with a Li/M/P molar ratio of 1:1:1.0 are severely

Table 1 Lattice parameters for samples hydrothermally synthesized with various molar ratios of Li/M/P and the pH value of reaction suspensions before hydrothermal synthesis

Li/M/P	a (Å)	b (Å)	c (Å)	V (Å^3)	pH
1:1:1.0	6.09035	10.44990	4.75271	302.48	10.51
1:1:1.2	6.09428	10.44980	4.75114	302.57	10.04
1:1:1.4	6.09079	10.43934	4.74815	301.90	9.82
1:1:1.6	6.08989	10.44129	4.74433	301.67	9.55
1:1:1.8	6.09010	10.44084	4.74514	301.72	9.39
1:1:2.0	6.09066	10.43978	4.74488	301.70	9.06

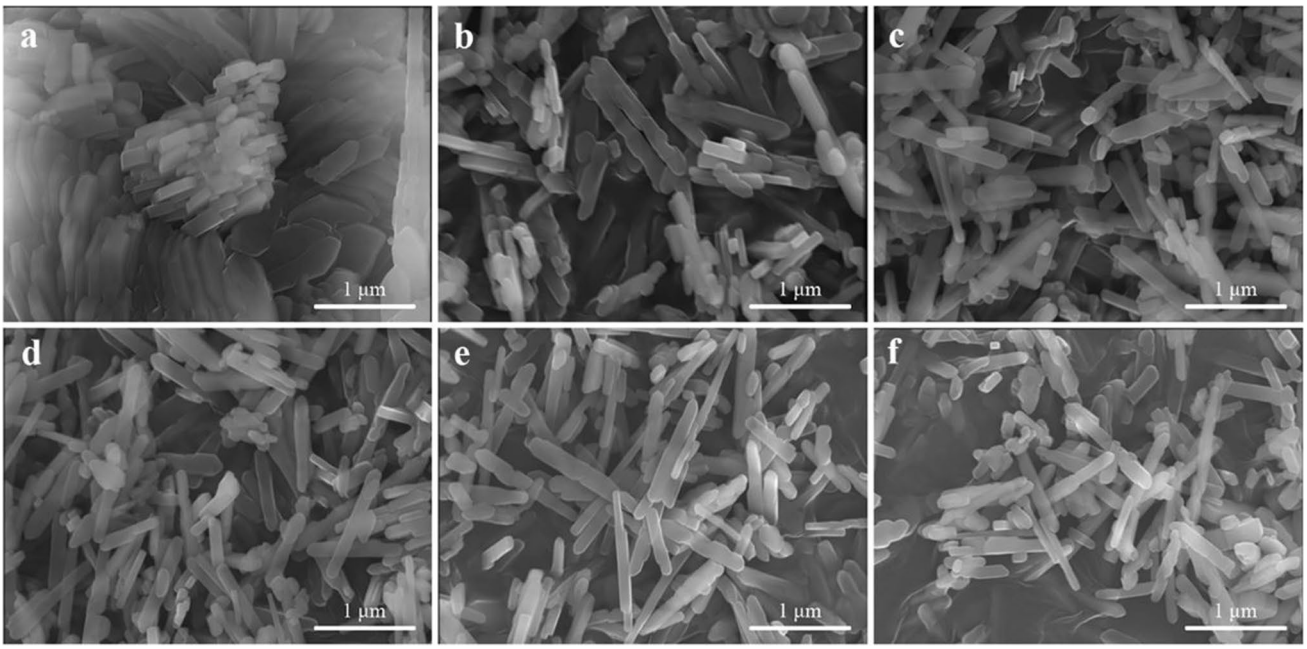

Fig. 3 SEM images of samples hydrothermally synthesized with various molar ratios of Li/M/P: **a** 1:1:1.0, **b** 1:1:1.2, **c** 1:1:1.4, **d** 1:1:1.6, **e** 1:1:1.8, and **f** 1:1:2.0

agglomerated, and the dispersion of particles is apparently improved with increasing P excess. From the above measurements, it is demonstrated that P excess not only can suppress the occurrence of undesirable oxidation reaction during hydrothermal synthesis, but also improve the dispersion of particles.

To evaluate the electrochemical performance of hydrothermal samples, the obtained samples were composited with carbon, and the capacity and rate are calculated without deducting the content of inactive carbon from the composite. The residual carbon content in all composites is about 5.1 wt.%. Figure 4a shows typical charge/discharge curves of all hydrothermal samples at 0.2 C. All curves exhibit two charge/discharge plateaus around 3.4 V (vs. Li^+/Li) for the Fe^{3+}/Fe^{2+} redox couple and 4.1 V (vs. Li^+/Li) for the Mn^{3+}/Mn^{2+} redox couple. The sample synthesized without P excess gives low capacity, and increased capacity and prolonged 3.4 V plateau are clearly observed when the samples synthesized with P excess of 1.2, 1.4, and 1.6, which also indicates that more Fe^{2+} was incorporated into the olivine structure on the condition of P excess. Meanwhile, it is noted that the samples synthesized with P excess of 1.6, 1.8, and 2.0 show almost the same charge/discharge curves with comparable capacity. Figures 4b and c compare rate and cycling performance of all samples. It is seen that all samples show good cycling performance but different rate capability is observed, and the samples synthesized with P excess can deliver higher capacities at high rates. Also, the samples synthesized with P excess of 1.6, 1.8, and 2.0 have a similar rate capability. For example, the sample synthesized with a Li/M/P molar ratio of 1:1:1.8 can deliver capacities of 146.6, 136.7, and 116 mAh g^{-1} at 0.1, 1, and 5 C, respectively. Moreover, EIS measurements were conducted at the fully discharged state after 5 cycles at 0.2 C, and the recorded EIS spectra are presented in Fig. 4d. The spectra of all samples consist of a semicircle in the high-to-medium-frequency region and an inclined line in the low-frequency region. The semicircle represents the charge transfer resistance (R_{ct}) and decreases with increasing P excess. In general, the three samples synthesized with P excess of 1.6, 1.8, and 2.0 have a comparable size of semicircles which are much smaller than those of other three samples. However, an additional arc in the intermediate frequency region is present in the spectrum of the sample synthesized with a Li/M/P molar ratio of 1:1:1.0 and becomes less obvious for the spectrum of the sample synthesized with a Li/M/P molar ratio of 1:1:1.2, and this interfacial impedance should be associated with the presence of iron oxide impurity in these two samples as revealed by XRD. In the low-frequency region, the inclined line represents the Warburg impedance associated with the Li^+ diffusion in the bulk of samples. It is well documented that there is an inverse relationship between the Li^+ diffusion coefficient $D_{Li}{}^+$ and the Warburg factor σ [51]. The Warburg factor σ is the slope between $\omega^{-1/2}$ and Z′ of the low-frequency region in Fig. 4e. The slopes are 178.45, 218.42, 147.02, 92.11, 87.88, and 104.56 for samples with

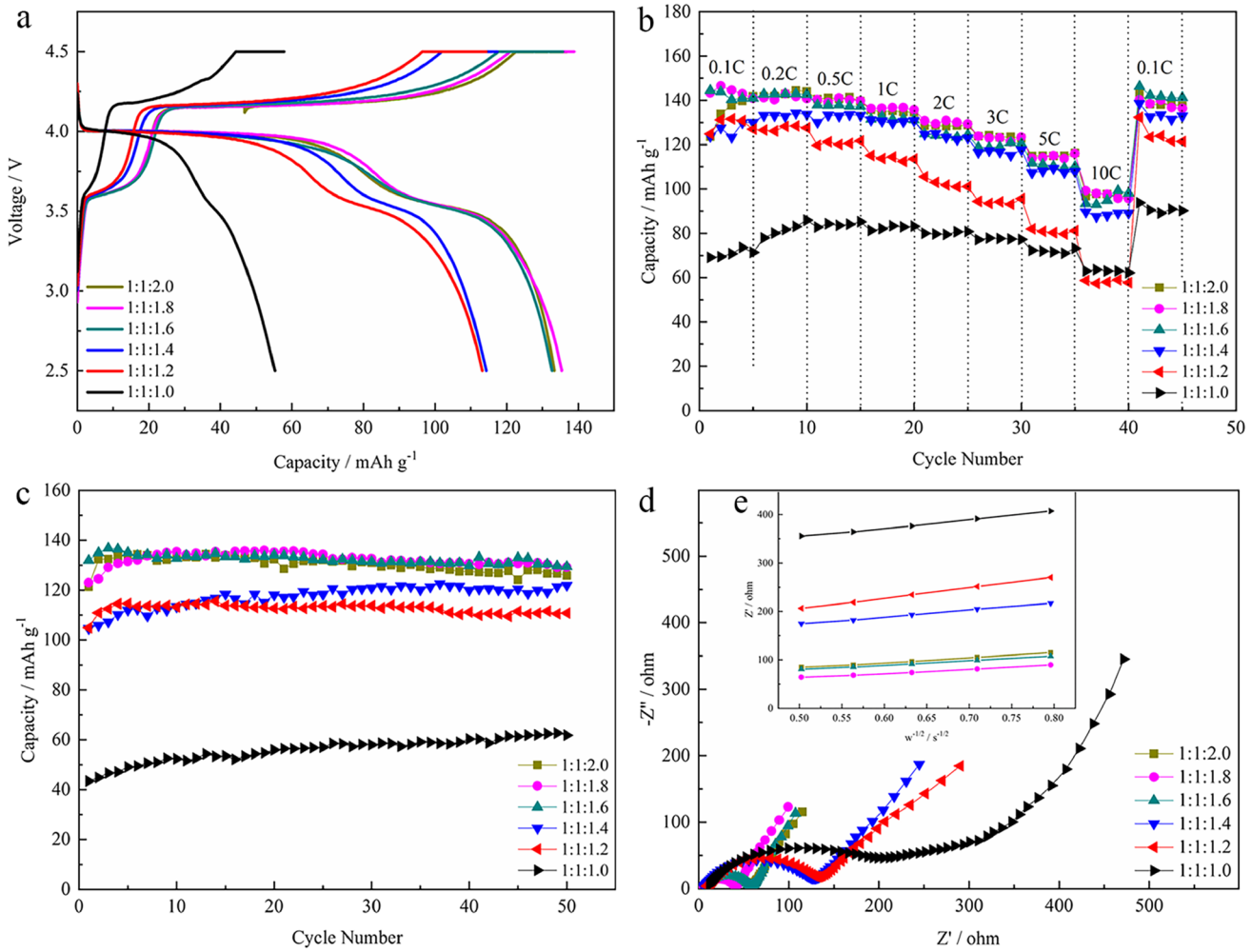

Fig. 4 **a** Charge/discharge curves at 0.2 C, **b** rate performance, **c** cycling performance at 0.2 C, **d** EIS spectra under fully discharged after 5 cycles at 0.2 C, and **e** the relationship between Z′ and $\omega^{-1/2}$ of $LiMn_{0.8}Fe_{0.19}Mg_{0.01}PO_4$/C samples hydrothermally synthesized with various molar ratios of Li/M/P

Li/M/P molar ratios of 1:1:1.0, 1:1:1.2, 1:1:1.4, 1:1:1.6, 1:1:1.8, and 1:1:2.0, respectively. The sample synthesized with a Li/M/P molar ratio of 1:1:1.8 has the minimum value of σ (87.88) and hence has the max Li^+ diffusion coefficient. The results of EIS measurement are well correlated with those of XRD, the charge/discharge measurements, and the results of these measurements all show that increasing P excess is conducive to hydrothermal synthesis and property of $LiMn_{0.8}Fe_{0.19}Mg_{0.01}PO_4$.

For the present hydrothermal synthesis in a P excess reaction system, increasing P excess is achieved by raising the amount of K_2HPO_4 which also gives rise to the pH variation of the reaction system, as shown in Table 1. Table 1 shows the pH value of reaction suspensions before hydrothermal synthesis. It is seen that the pH value decreases nearly linearly with increasing P excess, which indicates the accelerated ionization of HPO_4^-. This reminds us that the changes observed on hydrothermal synthesis of $LiMn_{0.8}Fe_{0.19}Mg_{0.01}PO_4$ with P excess may be resulted from pH variation. Therefore, in order to investigate the effect of pH on hydrothermal synthesis of $LiMn_{0.8}Fe_{0.19}Mg_{0.01}PO_4$, a series of samples were synthesized from reaction suspensions with the same Li/M/P molar ratio of 1:1:1.8, but the pH value of suspensions was adjusted by sulfuric acid or potassium hydroxide to 10.42, 10.11, 9.39, 8.71, and 8.61, respectively. From the representative photos of suspensions after hydrothermal synthesis (The change in the color of the suspension is shown in Fig. 1 and omitted here.), it can be clearly observed that with increasing the pH value, the suspension color changes gradually from milky white to yellowish brown. When the pH value increases to more than 10, the yellowish brown color of the suspension clearly indicates the

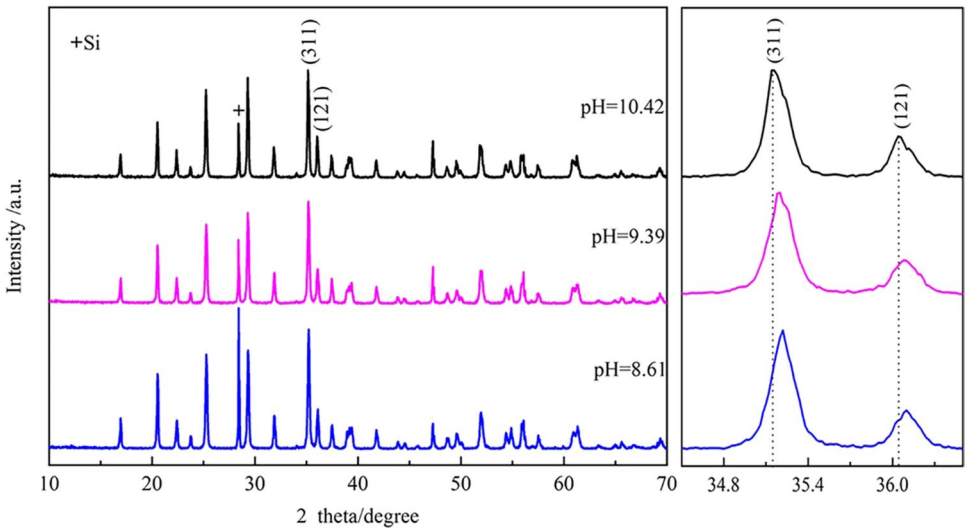

Fig. 5 XRD patterns of samples hydrothermally synthesized from suspensions with the same Li/M/P ratio of 1:1:1.8 and at various pH values

occurrence of undesirable oxidation reaction. Figure 5 shows three representative XRD patterns of samples synthesized from suspensions at pH values of 10.42, 9.39, and 8.61. All patterns can be indexed into an orthorhombic structure with a space group of *Pnma*, and no evidence of impurities is found. However, there is a slight shift of diffraction peaks to the higher angle with decreasing the pH value (peaks positions have been calibrated by internal standard of silicon), and the lattice parameters are calculated and listed in Table 2. It is clear that the lattice shrinks with the decrease of the pH value, also indicating that more Fe^{2+} is incorporated into material and the undesirable oxidation reaction is suppressed. According to the preceding analysis, oxidation impurity at pH = 10.42 is undetectable by XRD due to its amorphous state of the impurity, but the phenomenon of oxidation can be intuitively observed in representative photographs of the suspension after hydrothermal synthesis. These observations suggest that the undesirable oxidation reaction (Fe^{2+} oxidation) readily occurred at pH values above 10. Figure 6 shows SEM images of samples synthesized at pH values of 8.61, 9.39, and 10.42. The dispersion of these samples is similar, but the sample synthesized at the pH value of 10.42 has relatively larger particles.

Table 2 Lattice parameters of the samples hydrothermally synthesized from suspensions with the same Li/M/P ratio of 1:1:1.8 and at various pH values

pH	a (Å)	b (Å)	c (Å)	V (Å^3)
10.42	6.09244	10.45032	4.74979	302.41
9.39	6.09010	10.44084	4.74514	301.72
8.61	6.08611	10.43958	4.74154	301.38

Figure 7 compares the electrochemical performance of $LiMn_{0.8}Fe_{0.19}Mg_{0.01}PO_4$/C composites synthesized from suspensions with the same Li/M/P ratio of 1:1:1.8 and at various pH values. Clearly, the samples synthesized at pH values of 10.11 and 10.42 have poor performance, while the samples synthesized at pH values of 8.61, 8.71, and 9.39 show much better electrochemical performance. Figure 7d displays EIS spectra of these five samples. It is noted that the sample synthesized at the pH value of 10.42 presents a big additional arc in the intermediate-frequency region, and the sample synthesized at the pH value of 10.11 has a less obvious additional arc, which is associated to the additional interfacial impedance of iron oxide impurity. The other three spectra are free of the additional arc in the intermediate frequency region and have smaller R_{ct} and the higher Li^+ diffusion rate (Fig. 7e). The results of all measurements are well correlated and show that the pH value of hydrothermal suspension has an apparent influence on the hydrothermal synthesis and property of the product. The above studies indicate that the undesirable Fe^{2+} oxidation reaction takes place readily when the pH value of hydrothermal suspension is higher than 10, which is harmful for hydrothermal synthesis of $LiMn_{0.8}Fe_{0.19}Mg_{0.01}PO_4$.

Now the question is whether the excess P really plays a role in the hydrothermal synthesis. To address this question, the influence of the pH should be eliminated when the degree of P excess is varied in the suspension. Herein, additional samples were synthesized from suspensions at almost the same pH value of 9.4 but with different P excess. The suspensions with Li/M/P molar ratios of 1:1:1.0 and 1:1:1.2 were both adjusted to a pH value of 9.4 by addition of sulfuric acid before hydrothermal reaction. This pH value is almost the same as that (9.39) of the suspension with the Li/M/P molar

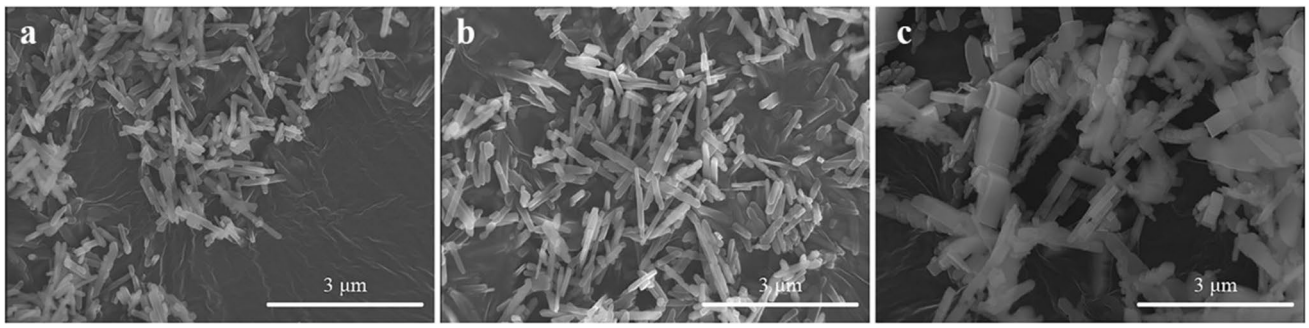

Fig. 6 SEM images of the samples hydrothermally synthesized from suspensions with the same Li/M/P ratio of 1:1:1.8 and at various pH values: **a** 8.61, **b** 9.39, and **c** 10.42

ratio of 1:1:1.8. The representative photos of these suspensions (with almost the same pH value of 9.4 before hydrothermal reaction) after hydrothermal synthesis with different Li/M/P molar ratios were also observed. With increasing P excess, the color of suspension becomes light, which is similar to what was observed

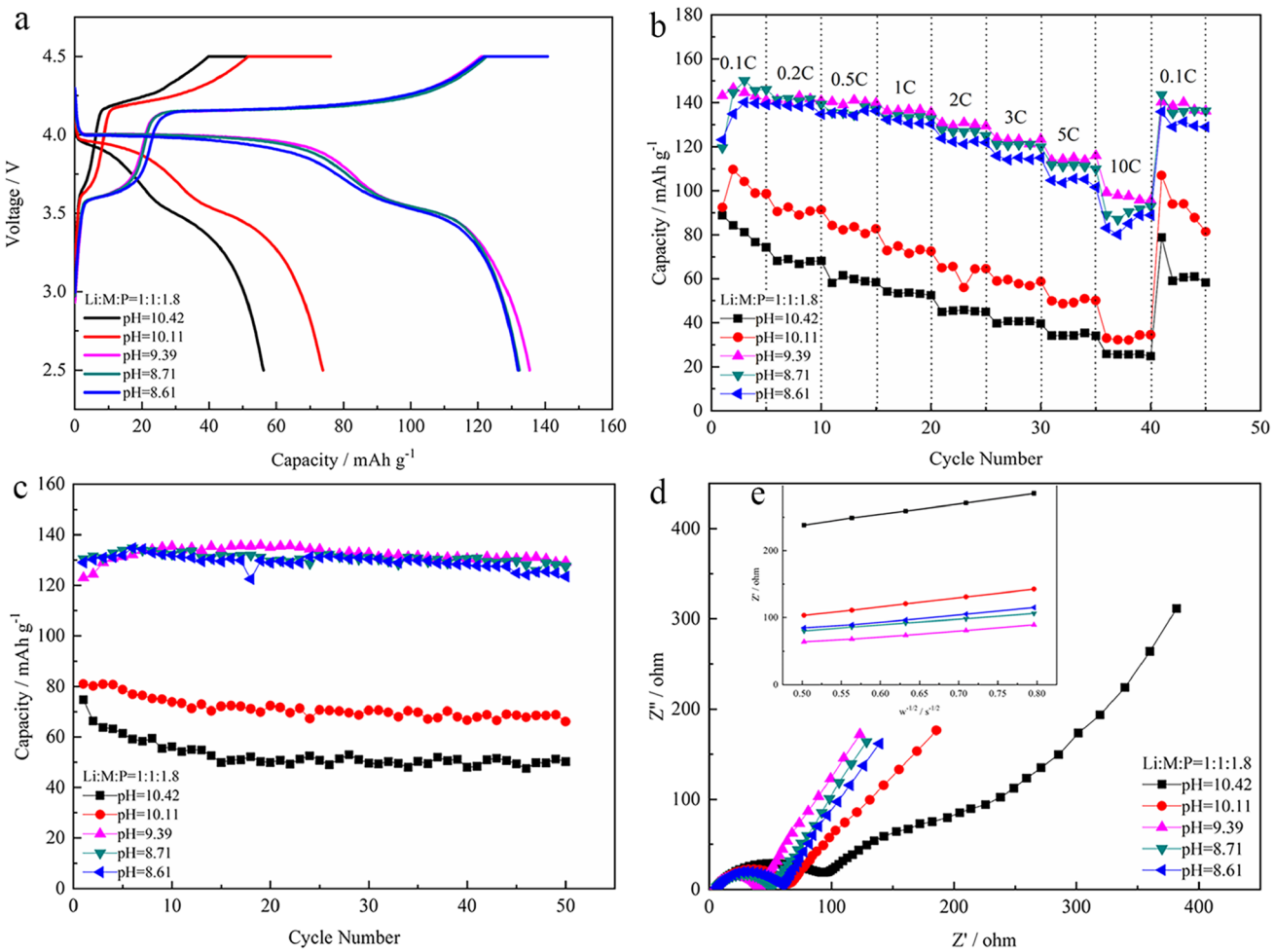

Fig. 7 **a** Charge/discharge curves at 0.2 C, **b** rate performance, **c** cycling performance at 0.2 C, **d** EIS spectra under fully discharged after 5 cycles at 0.2 C, and **e** the relationship between Z′ and $\omega^{-1/2}$ of $LiMn_{0.8}Fe_{0.19}Mg_{0.01}PO_4$/C samples hydrothermally synthesized from suspensions with the same Li/M/P ratio of 1:1:1.8 and at various pH values

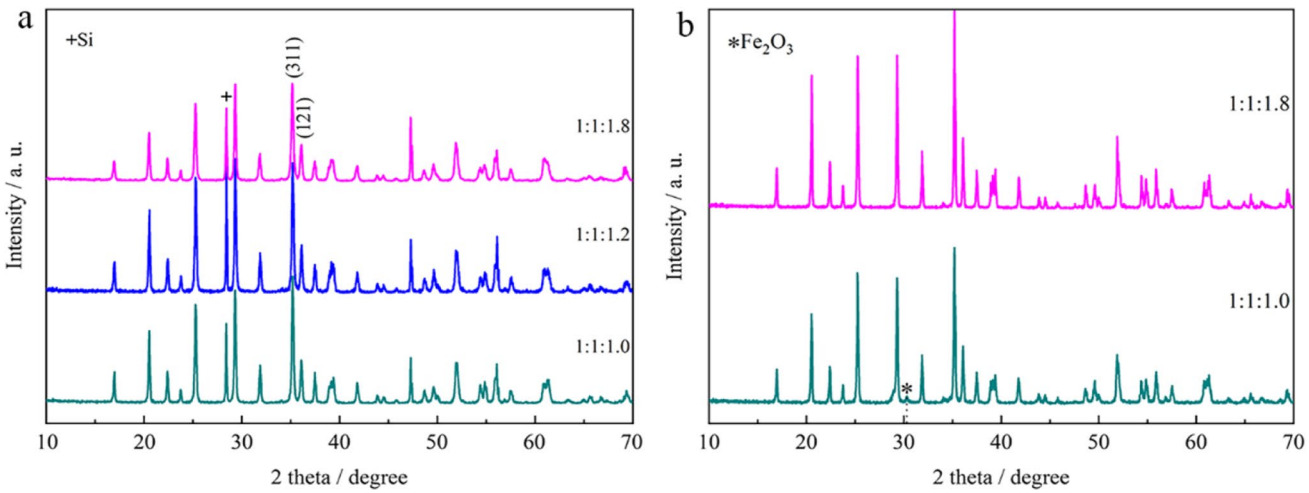

Fig. 8 **a** XRD patterns of samples hydrothermally synthesized from suspensions (at almost the same pH value of 9.4 before hydrothermal reaction) with various Li/M/P molar ratios and **b** XRD patterns of samples post-annealed at 600 °C for 1 h under a nitrogen atmosphere

in Fig. 1, and is related to the occurrence of undesirable oxidation reaction. Figure 8 shows the XRD patterns of the samples (peaks positions have been calibrated by internal standard of silicon). All samples are orthorhombic structures with a *Pnma* space group, and no impurity peaks are detected. Figure 8b shows the XRD patterns of the samples with Li/M/P molar ratios of 1:1:1.0 and 1:1:1.8 after post-annealing at 600 °C for 1 h under a nitrogen atmosphere, and a tiny diffraction peak of Fe_2O_3 impurity (indicated by asterisk) can be observed in the XRD pattern of the sample without P excess. Apparently, these observations prove that increasing P excess can suppress the occurrence of undesirable oxidation (such as Fe^{2+} oxidation). Figure 9 shows SEM images of these samples. It is seen that particles of the sample synthesized with a Li/M/P molar ratio of 1:1:1.0 are seriously agglomerated, and the agglomeration of particles is significantly reduced with increasing P excess. It is confirmed that excess P can improve particles dispersion of the hydrothermal sample.

The electrochemical performance of these samples is shown in Fig. 10. Compared with the two samples synthesized with Li/M/P molar ratios of 1:1:1.0 and 1:1:1.2, the sample synthesized with the Li/M/P molar ratio of 1:1:1.8 gives much better electrochemical performance, smaller R_{ct}, and higher Li^+ diffusion rate (from Fig. 10e, the slope is 122.59, 127.22, and 87.88 for samples synthesized with Li/M/P molar ratios of 1:1:1.0, 1:1:1.2, and 1:1:1.8, respectively). In short, the results of these additional experiments confirm that P excess is indeed beneficial to the hydrothermal synthesis of $LiMn_{0.8}Fe_{0.19}Mg_{0.01}PO_4$, including suppressing the occurrence of undesirable Fe^{2+} oxidation reaction and improving the particle dispersion,

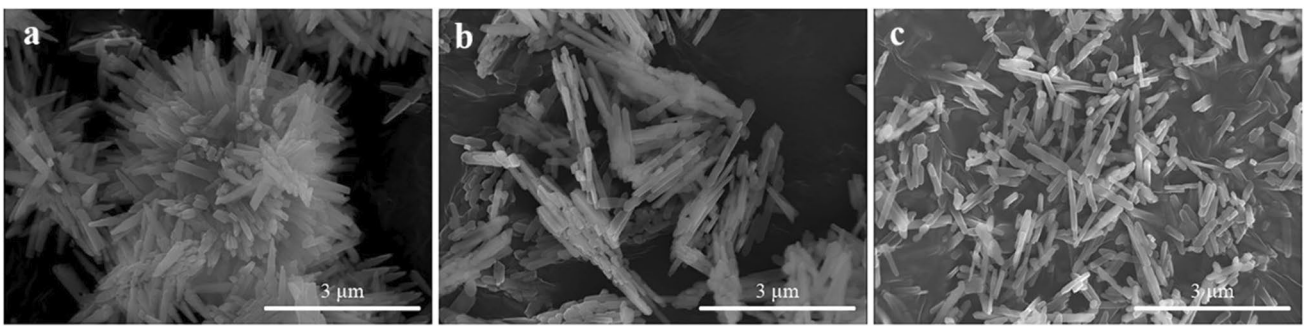

Fig. 9 SEM images of samples hydrothermally synthesized from suspensions (at almost the same pH value of 9.4 before hydrothermal reaction) with various Li/M/P molar ratios: **a** 1:1:1.0, **b** 1:1:1.2, and **c** 1:1:1.8

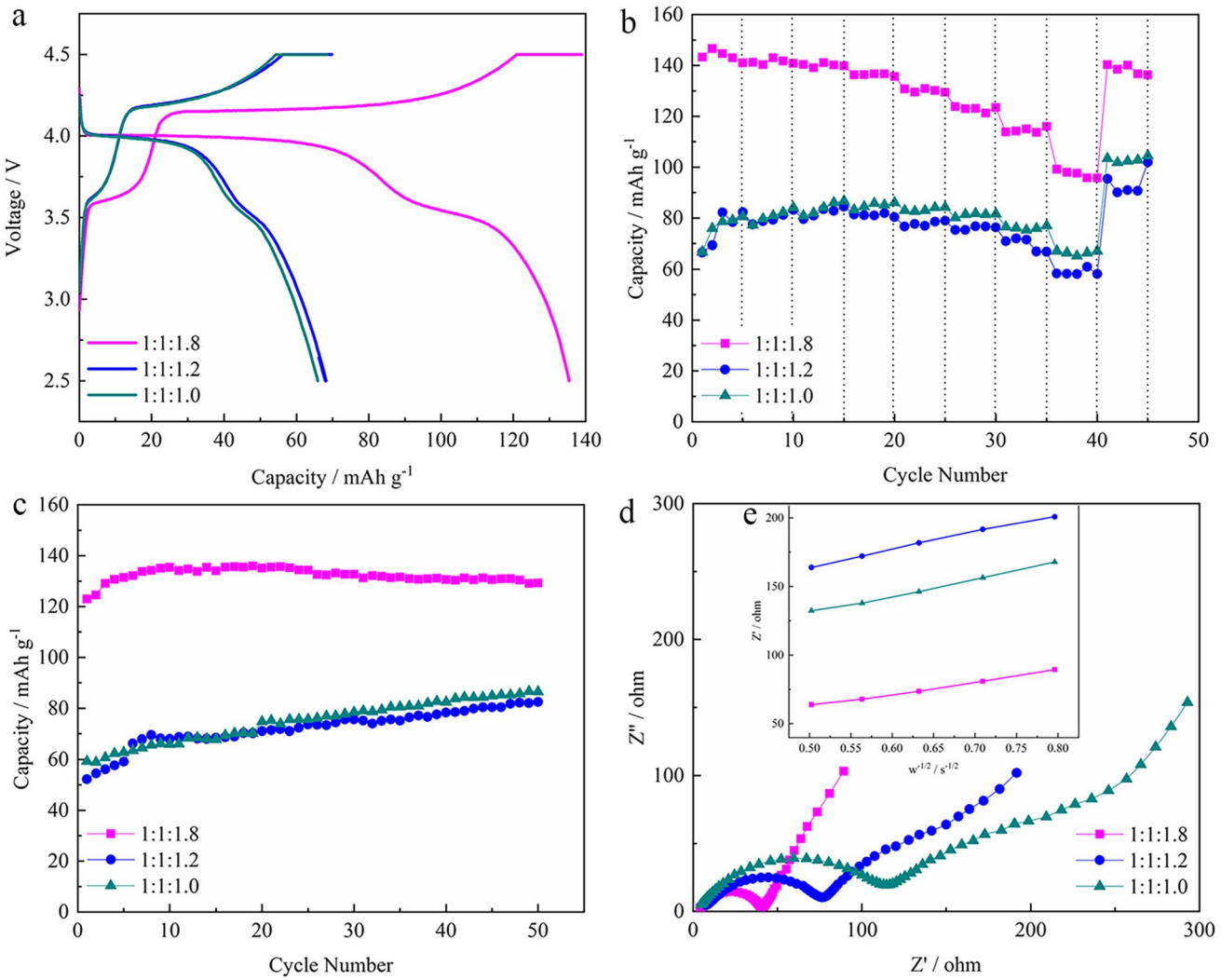

Fig. 10 **a** Charge/discharge curves at 0.2 C, **b** rate performance, **c** cycling performance at 0.2 C, **d** EIS spectra under fully discharged state after 5 cycles at 0.2 C, and **e** the relationship between Z′ and $\omega^{-1/2}$ of $LiMn_{0.8}Fe_{0.19}Mg_{0.01}PO_4$/C samples hydrothermally synthesized from suspensions (at almost the same pH value of 9.4 before hydrothermal reaction) with various Li/M/P molar ratios

which give rise to significantly improved electrochemical performance of hydrothermal samples.

Conclusions

In this paper, a series of $LiMn_{0.8}Fe_{0.19}Mg_{0.01}PO_4$ samples are hydrothermally synthesized from the P excess reaction system, and the effect of P excess was studied in detail. Our results show that varying the degree of P excess accompanies changed pH value of the reaction suspension, which can alter the stability of Fe^{2+} in the suspension and the particle dispersion of the hydrothermal product. When the degree of P excess is fixed, the pH values exceeding 10 is negative to hydrothermal synthesis due to the occurrence of undesirable Fe^{2+}oxidation and increased particles, which lead to poor performance. When the pH value remains constant, increasing P excess can suppress the occurrence of undesired Fe^{2+}oxidation during hydrothermal synthesis and improve the particles dispersion, which can significantly improve the electrochemical performance of the hydrothermal sample. In conclusion, a proper degree of P excess can improve the hydrothermal synthesis of $LiMn_{0.8}Fe_{0.19}Mg_{0.01}PO_4$, and much better electrochemical performance can be achieved for the obtained product. These effects of P excess should be general and applicable to hydrothermal synthesis of other lithium transition metal phosphates.

Funding This work is supported by the National Natural Science Foundation of China (grant numbers 51874155 and 51664031).

Declarations

Conflict of Interest The authors declare no conflict of interest.

References

1. Yoshimura M (1998) Importance of soft solution processing for advanced inorganic materials. J Mater Res 13:796–802
2. Demazeau G (1999) Solvothermal processes: a route to the stabilization of new materials. J Mater Chem 9:15–18
3. Yu SH (2001) Hydrothermal/solvothermal processing of advanced ceramic materials. J Ceram Soc Jpn 109:S65–S75
4. Cushing BL, Kolesnichenko VL, O'Connor CJ (2004) Recent advances in the liquid-phase syntheses of inorganic nanoparticles. Chem Rev 104:3893–3946
5. Whittingham MS (2004) Lithium batteries and cathode materials. Chem Rev 104:4271–4301
6. Devaraju MK, Honma I (2012) Hydrothermal and solvothermal process towards development of $LiMPO_4$ (M = Fe, Mn) nanomaterials for lithium-ion batteries. Adv Energy Mater 2:284–297
7. Devaraju MK, Truong QD, Tomai T, Honma I (2014) Supercritical fluid methods for synthesizing cathode materials towards lithium ion battery applications. Rsc Adv 4:27452–27470
8. Zhang J, Luo SH, Chang LJ, Bao S, Liu JN, Hao AM, Wang ZY, Liu YG, Xu Q, Zhai YC (2016) In-situ growth of $LiMnPO_4$ on porous $LiAlO_2$ nanoplates substrates from AAO synthesized by hydrothermal reaction with improved electrochemical performance. Electrochim Acta 193:6–23
9. Luo SH, Hu DB, Liu H, Li JZ, Yi TF (2019) Hydrothermal synthesis and characterization of α-Fe_2O_3/C using acid-pickled iron oxide red for Li-ion batteries. J Hazard Mater 368:714–721
10. Li JZ, Luo SH, Sun Y, Li JY, Zhang J, Yi TF (2019) $Li_{0.95}Na_{0.05}MnPO_4$/C nanoparticles compounded with reduced graphene oxide sheets for superior lithium ion battery cathode performance. Ceram Int 45:4849–4856
11. Padhi AK, Nanjundaswamy KS, Goodenough JB (1997) Phospho-olivines as positive-electrode materials for rechargeable lithium batteries. J Electrochem Soc 144:1188–1194
12. Ravet N, Chouinard Y, Magnan JF, Besner S, Gauthier M, Armand M (2001) Electroactivity of natural or synthetic triphylite. J Power Sources 97–98:503–507
13. Chen ZH, Dahn JR (2002) Reducing carbon in $LiFePO_4$/C composite electrodes to maximize specific energy, volumetric energy, and tap density. J Electrochem Soc 149:A1184–A1189
14. Chung SY, Bloking JT, Chiang YM (2002) Electronically conductive phospho-olivines as lithium storage electrodes. Nat Mater 1:123–128
15. Li GH, Azuma H, Tohda M (2002) $LiMnPO_4$ as the cathode for lithium batteries. Electrochem Solid-State Lett 5:A135–A137
16. Yamada A, Hosoya M, Chung SC, Kudo Y, Hinokuma K, Liu KY, Nishi Y (2003) Olivine-type cathodes: achievements and problems. J Power Sources 119–121:232–238
17. Herle PS, Ellis B, Coombs N, Nazar LF (2004) Nano-network electronic conduction in iron and nickel olivine phosphates. Nat Mater 3:147–152
18. Islam MS, Driscoll DJ, Fisher CAJ, Slater PR (2005) Atomic-scale investigation of defects, dopants, and lithium transport in the $LiFePO_4$ olivine-type battery material. Chem Mater 17:5085–5092
19. Delacourt C, Poizot P, Levasseur S, Masquelier C (2006) Size effects on carbon-free $LiFePO_4$ powders: the key to superior energy density. Electrochem Solid-State Lett 9:A352–A355
20. Gibot P, Casa-Cabanas M, Laffont L, Levasseur S, Carlach P, Hamelet S, Tarascon JM, Masquelier C (2008) Room-temperature single-phase Li insertion/extraction in nanoscale Li_xFePO_4. Nat Mater 7:741–747
21. Fisher CAJ, Prieto VMH, Islam MS (2008) Lithium battery materials LiMPO4 (M = Mn, Fe Co, and Ni): insights into defect association, transport mechanisms, and doping behavior. Chem Mater 20:5907–5915
22. Martha SK, Grinblat J, Haik O, Zinigrad E, Drezen T, Miners JH, Exnar I, Kay A, Markovsky B, Aurbach D (2009) $LiMn_{0.8}Fe_{0.2}PO_4$: an advanced cathode material for rechargeable lithium batteries. Angew Chem Int Ed 48:8559–8563
23. Oh SM, Oh SW, Yoon CS, Scrosati B, Amine K, Sun YK (2010) High-performance carbon-$LiMnPO_4$ nanocomposite cathode for lithium batteries. Adv Funct Mater 20:3260–3265
24. Hu CL, Yi HH, Fang HS, Yang B, Yao YC, Ma WH, Dai YN (2010) Improving the electrochemical activity of $LiMnPO_4$ via Mn-site co-substitution with Fe and Mg. Electrochem Commun 12:1784–1787
25. Fang HS, Dai ER, Yang B, Yao YC, Ma WH (2012) $LiMn_{0.8}Fe_{0.19}Mg_{0.01}PO_4$/C as a high performance cathode material for lithium ion batteries. J Power Sources 204:193–196
26. Liu S, Fang HS, Dai ER, Yang B, Yao YC, Ma WH, Dai YN (2014) Effect of carbon content on properties of $LiMn_{0.8}Fe_{0.19}Mg_{0.01}PO_4$/C composite cathode for lithium ion batteries. Electrochim Acta 116:97–102
27. Zhang XY, van Hulzen M, Singh DP, Brownrigg A, Wright JP, van Dijk NH, Wagemaker M (2015) Direct view on the phase evolution in individual $LiFePO_4$ nanoparticles during Li-ion battery cycling. Nat Commun 6:8333
28. Hong L, Li LS, Chen-Wiegart YK, Wang JJ, Xiang K, Gan LY, Li WJ, Meng F, Wang F, Wang J, Chiang YM, Jin S, Tang M (2017) Two-dimensional lithium diffusion behavior and probable hybrid phase transformation kinetics in olivine lithium iron phosphate. Nat Commun 8:114
29. Kobayashi S, Kuwabara A, Fisher CAJ, Ukyo Y, Ikuhara Y (2018) Microscopic mechanism of biphasic interface relaxation in lithium iron phosphate after delithiation. Nat Commun 9:2863
30. Khalfaouy RE, Turan S, Dermenci KB, Savaci U, Addaou A, Laajeb A, Lahsini A (2019) Nickel-substituted $LiMnPO_4$/C olivine cathode material: Combustion synthesis, characterization and electrochemical performances. Ceram Int 45:17688–17695
31. Chen W, Fang HS (2019) Aluminum doping in $LiMnPO_4$ with an unexpected charge compensation. J Electrochem Soc 166:A2752–A2754
32. Manthiram A (2020) A reflection on lithium-ion battery cathode chemistry. Nat Commun 11:1
33. Yang SF, Zavalij PY, Whittingham MS (2001) Hydrothermal synthesis of lithium iron phosphate cathodes. Electrochem Commun 3:505–508
34. Chen JJ, Wang SJ, Whittingham MS (2007) Hydrothermal synthesis of cathode materials. J Power Sources 174:442–448
35. Tajimi S, Ikeda Y, Uematsu K, Toda K, Sato M (2004) Enhanced electrochemical performance of $LiFePO_4$ prepared by hydrothermal reaction. Solid State Ionics 175:287–290
36. Meligrana G, Gerbaldi C, Tuel A, Bodoardo S, Penazzi N (2006) Hydrothermal synthesis of high surface $LiFePO_4$ powers as cathode for Li-ion cells. J Power Sources 160:516–522
37. Dokko K, Shiraishi K, Kanamura K (2005) Identification of surface impurities on $LiFePO_4$ particles prepared by a hydrothermal process. J Chem Soc 152:A2199-2202
38. Dokko K, Koizumi S, Nakano H, Kanamura K (2007) Particle morphology, crystal orientation, and electrochemical reactivity of $LiFePO_4$ synthesized by the hydrothermal method at 443 K. J Mater Chem 17:4803–4810

39. Ellis B, Kan WH, Makahnouk WRM, Nazar LF (2007) Synthesis of nanocrystals and morphology control of hydrothermal prepared $LiFePO_4$. J Mater Chem 17:3248–3254
40. Fang HS, Pan ZY, Li LP, Yang Y, Yan GF, Li GS, Wei SQ (2008) The possibility of manganese disorder in $LiMnPO_4$ and its effect on the electrochemical activity. Electrochem Commun 10:1071–1073
41. Jugović D, Uskoković D (2009) A review of recent developments in the synthesis procedures of lithium iron phosphate powders. J Power Sources 190:538–544
42. Bo J, Gu HB, Zhang W, Park KH, Sun GP (2008) Effect of different carbon conductive additives on electrochemical properties of $LiFePO_4$-C/Li batteries. J Solid State Electrochem 12:1549–1554
43. Zhao RR, Lan BY, Chen HY, Ma GZ (2012) Hydrothermal synthesis and properties of manganese-doped $LiFePO_4$. Ionics 18:873–879
44. Zhang N, Lin L, Xu Z (2014) Effect of synthesis temperature, time, and carbon content on the properties and lithium-ion diffusion of $LiFePO_4$/C composites. J Solid State Electrochem 18:2401–2410
45. Muruganantham R, Sivakumar M, Subadevi R (2016) Synthesis and electrochemical characterization of olivine-type lithium iron phosphate cathode materials via different techniques. Ionics 22:1557–1565
46. Zhang JL, Wang J, Liu YY, Nie N, Gu JJ, Yu F, Li W (2015) High-performance lithium iron phosphate with phosphorus-doped carbon layers for lithium ion batteries. J Mater Chem A 3:2043–2049
47. Yang JX, Li ZJ, Guang TJ, Hu MM, Cheng RF, Wang RY, Shi C, Chen JX, Hou PX, Zhu KJ, Wang XH (2018) Green synthesis of high-performance $LiFePO_4$ nanocrystals in pure water. Green Chem 20:5215–5223
48. Qin X, Wang JM, Xie J, Li FZ, Wen L, Wang XH (2012) Hydrothermally synthesized $LiFePO_4$ crystals with enhanced electrochemical properties: simultaneous suppression of crystal growth along [010] and antisite defect formation. Phys Chem Chem Phys 14:2669–2677
49. Lee J, Teja AS (2005) Characteristics of lithium iron phosphate ($LiFePO_4$) particles synthesized in subcritical and supercritical water. J Supercrit Fluids 35:83–90
50. Li LM, Lu XP, Chen W, Fang HS (2019) A new strategy to hydrothermally synthesize olivine phosphates. Chem Commun 55:12092–12095
51. Liu H, Li C, Zhang HP, Fu LJ, Wu YP, Wu HQ (2006) Kinetic study on $LiFePO_4$/C nanocomposites synthesized by solid state technique. J Power Sources 159:717–720